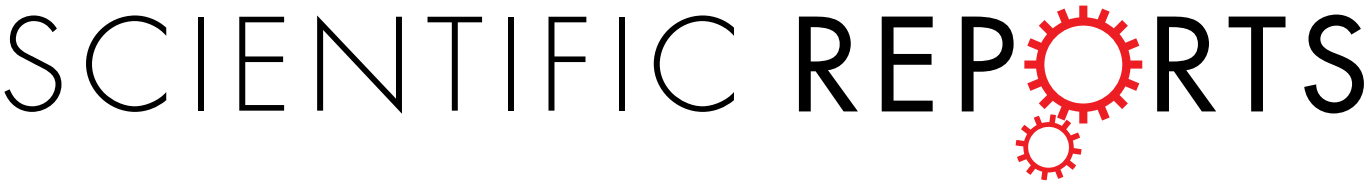

OPEN

Control of Radiative Exciton Recombination by Charge Transfer Induced Surface Dipoles in MoS_2 and WS_2 Monolayers

Received: 15 November 2015
Accepted: 21 March 2016
Published: 07 April 2016

Peng Hu[1], Jun Ye[2], Xuexia He[1], Kezhao Du[1], Keke K. Zhang[1], Xingzhi Wang[3], Qihua Xiong[3], Zheng Liu[1], Hui Jiang[1] & Christian Kloc[1]

Due to the two dimensional confinement of electrons in a monolayer of 2D materials, the properties of monolayer can be controlled by electrical field formed on the monolayer surface. F_4TCNQ was evaporated on MoS_2 and WS_2 monolayer forming dipoles between strong acceptor, F_4TCNQ, and monolayers of MoS_2 or WS_2. The strong acceptor attracts electrons (charge transfer) and decreases the number of the ionized excitons. Free excitons undergo radiative recombination in both MoS_2 and WS_2. Moreover, the photoluminescence enhancement is stronger in WS_2 where the exciton-phonon coupling is weaker. The theoretical model indicates that the surface dipole controls the radiative exciton recombination and enhances photoluminescence radiation. Deposition of F_4TCNQ on the 2D monolayers enables a convenient control of the radiative exciton recombination and leads to the applications of these materials in lasers or LEDs.

When an exciton, a quasiparticle consisting of an electron and a hole bound together by simple Coulomb interaction, recombines, i) photoluminescence occurs in the case of weak exciton-phonon coupling or ii) exciton recombines radiation-less increasing the phonon energy if this coupling is strong. In a monolayer of transition metal dichalcogenides (TMD), or a two dimensional electron gas, excitons can interact with free electrons forming charged excitons also known as trions, quasiparticles composed of two electrons and a hole[1]. Due to the presence of these tightly bound negative trions, the number of non-bounded excitons available for radiative recombination is limited and the photoluminescence is suppressed. In other words, the non-bounded excitons cannot radiative recombine producing photon (light) because they are bonded with free electrons forming trions[2–6]. Therefore, to increase the photoluminescence, the concentration of trions needs to be reduced. A strong electrical field formed by gate electrode on the two-dimensional (2D) layer of TMD or dipoles on the surface of TMD monolayer can reduce the trion concentration[1].

In previous studies, a chemical doping method was used to enhance the photoluminescence by interaction of TMD monolayer with acceptor in solvent[2,5]. Furthermore, some reports studied PL and optical properties controlled by the charge transfer between MoS_2 and metal nanoparticle[7] or graphene quantum dots[8]. It was shown that not only the PL intensity has been changed, but also the phase transition in MoS_2 monolayer is caused by charge transfer[9]. In this work, we evaporate 2,3,5,6-tetrafluoro-7,7,8,8-tetracyanoquinodimethane (F_4TCNQ) on TMD monolayer forming dipoles between strong acceptor, F_4TCNQ and monolayers of MoS_2 or WS_2. The strong acceptor attracts electrons (charge transfer) and decreases the number of the ionized excitons. Free excitons undergo radiative recombination in both MoS_2 and WS_2. Moreover, the photoluminescence enhancement is stronger in WS_2 where the exciton-phonon coupling is weaker. No solvent was used, which provide a clean system to compare to theoretical calculations. The theoretical model indicates that the surface dipole is controlling the radiative exciton recombination, which further increases the photoluminescence.

[1]School of Materials Science and Engineering, Nanyang Technological University, 639798 Singapore. [2]Institute of High Performance Computing, Agency for Science, Technology and Research, 138632 Singapore. [3]School of Physical and Mathematical Sciences, Nanyang Technological University, 637371 Singapore. Correspondence and requests for materials should be addressed to Z.L. (email: z.liu@ntu.edu.sg) or H.J. (email: jianghui@ntu.edu.sg) or C.K. (email: ckloc@ntu.edu.sg)

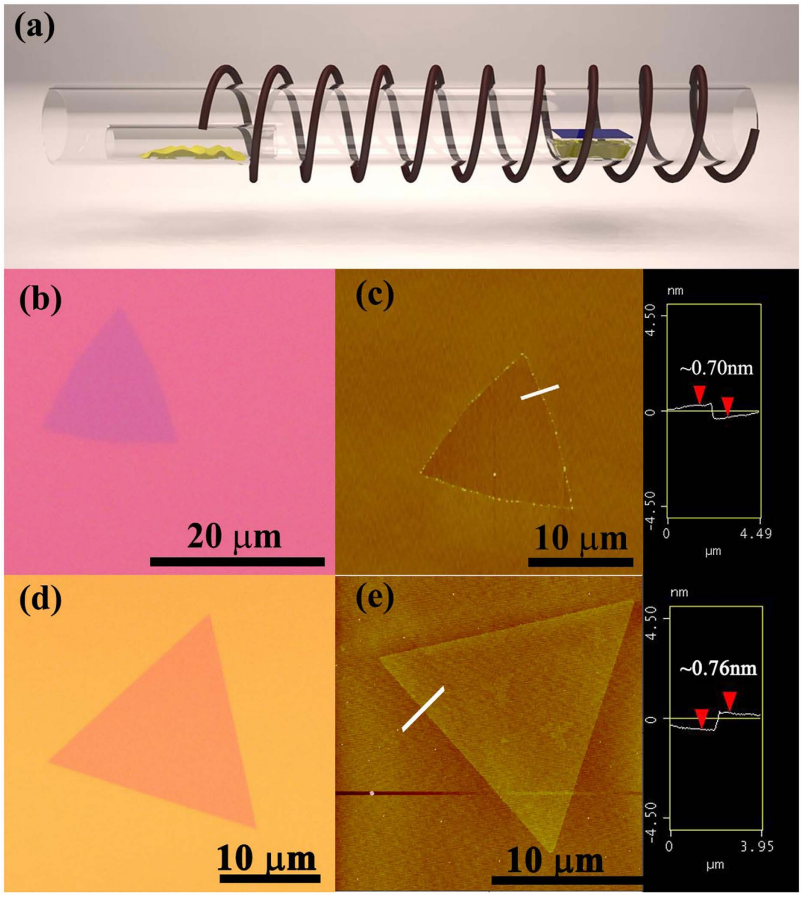

Figure 1. (**a**) Monolayer WS_2 and MoS_2 growth apparatus. (**b**) Optical image of triangle monolayer WS_2. (**c**) AFM image of a monolayer WS_2 on a SiO_2/Si substrate and the corresponding section analysis. (**d**) Optical image of triangle monolayer MoS_2. (**e**) AFM image of a monolayer MoS_2 on a SiO_2/Si substrate and the corresponding section analysis.

Results

MoS_2 and WS_2 monolayer growth and characterization. A triangle monolayer of WS_2 and MoS_2 was grown with the chemical vapor deposition (CVD) method onto a SiO_2/Si wafer. The monolayer growth apparatus is shown in Fig. 1(a). Triangular WS_2 and MoS_2 were grown at random locations on the substrate. Figure 1(b,d) show the optical images of the WS_2 and MoS_2, respectively. The thickness of the WS_2 and MoS_2 was determined by atomic force microscopy (AFM), as shown in Fig. 1(c,e). The AFM images indicate that both the WS_2 and MoS_2 have a smooth surface. The cross section height of the WS_2 and MoS_2 is approximately 0.70 nm and 0.76 nm, respectively, which corresponds to the monolayers of WS_2 [5,10] and MoS_2 [11–14].

The monolayer structure of WS_2 and MoS_2 is further confirmed by the Raman spectrum shown in Fig. 2. The E_{2g}^1 and A_{1g} modes of monolayer WS_2 are located at approximately 355 and 417 cm^{-1}, respectively[15–18]. With the number of layers increased, the in-plane vibrational E_{2g}^1 is slightly red-shifted, and the out-of-plane A_{1g} mode is blue-shifted. The energy difference between the Raman E_{2g}^1 and A_{1g} modes increased with the layer number. Thus, the energy difference can be used to identify the number of layers of WS_2. The energy difference shown in Fig. 2(a) is 62.5 cm^{-1}, which coincides with previous reports for monolayer WS_2 [15,19]. The same phenomenon is also observed in monolayer MoS_2. The in-plane vibrational E_{2g}^1 phonon mode is ~385 cm^{-1}, and the out-of-plane A_{1g} mode is ~404 cm^{-1}. The energy difference between the two modes is also dependent on the number of layers of MoS_2. The energy difference between the two modes is 18.2 cm^{-1}, as shown in Fig. 2(b), indicating that the MoS_2 is a monolayer[2,14,17,20,21].

Photoluminescence intensity after F_4TCNQ was deposited onto monolayer MoS_2/WS_2. Figure 3(a) shows that the PL intensity before and after F_4TCNQ was deposited onto monolayer WS_2. The PL intensity is approximately fifty times higher after the F_4TCNQ deposition. The position of the PL peak of monolayer WS_2 is slightly blue-shifted, while the peak shape did not change, as shown in Fig. 3(b). The PL intensity is also increased by approximately ten times after the F_4TCNQ is deposited on MoS_2 monolayer. The positon of the peak is also slightly blue-shifted, but the shape is not changed, as is shown in Fig. 3(c,d).

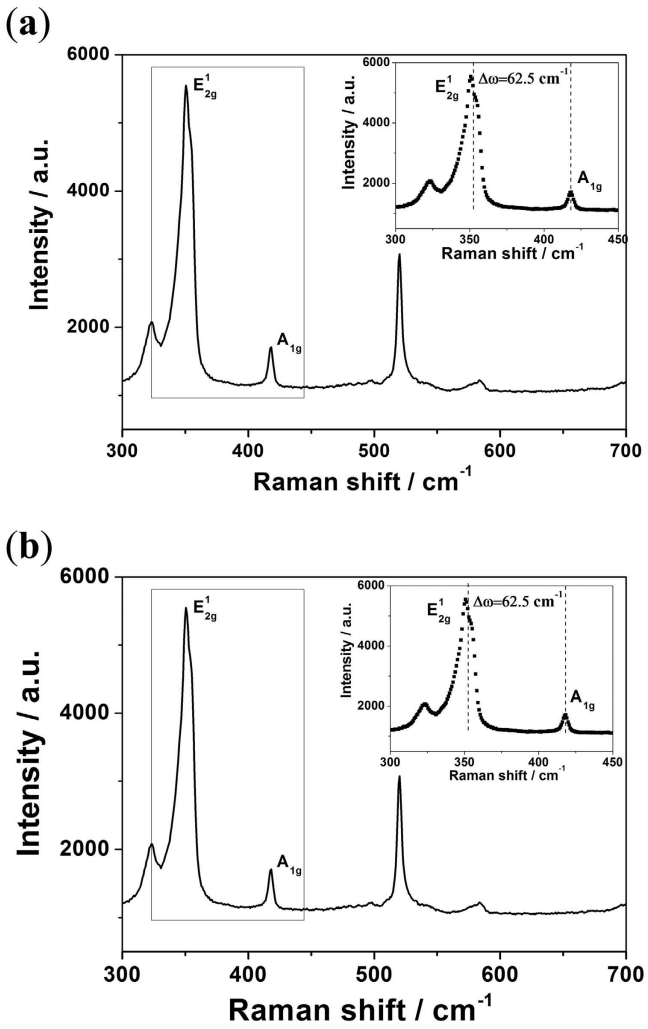

Figure 2. Raman spectra of a CVD-grown WS_2 monolayer (**a**) and MoS_2 monolayer (**b**). The inset shows the energy difference between the Raman $E_{2g}{}^1$ and A_{1g} modes.

Discussion

To understand the charge transfer from MoS_2/WS_2 to F_4TCNQ, we performed density functional (DFT) calculations[22] on the model systems shown in Fig. 4. In both the F_4TCNQ-doped MoS_2 and WS_2 cases, electron density depletion (as indicated by the white isosurfaces) were found in the interface regions where the nitrogen atoms in the F_4TCNQ molecules are closest to the surface sulfur atoms in MoS_2 and WS_2, as shown in Fig. 4(a,c), respectively. The electron density depletion in the MoS_2 layer is slightly greater than that in the WS_2 layer according to the electron density difference plots. An electron density increase (red isosurfaces) is observed on the F_4TCNQ molecules in both cases, as shown in Fig. 4(a,c). Charge transfer occurs around the interface regions in both cases. The energy level of F_4TCNQ and MoS_2/WS_2 are shown in Supporting Information - Figure S1. In addition, the barycenters of the holes (white isosurfaces) shown in Fig. 4(b,d) clearly suggest that the holes are close to the MoS_2 and WS_2 surfaces, indicating the charge transfer from MoS_2 or WS_2 to F_4TCNQ. The charge transfer distance (D_{CT}) between MoS_2 and F_4TCNQ (calculated $D_{CT} = 1.299$ Å) is shorter than that between WS_2 and F_4TCNQ (calculated $D_{CT} = 1.391$ Å). However the charge transfer direction, indicated by arrows on the Fig. 4(b,d) is determined by the orientation of F_4TCNQ molecule relative to the surface of the TMD monolayer.

According to our discussion in introduction, the charge transfer between MoS_2 or WS_2 monolayer and acceptor, F_4TCNQ forms dipole layers at interface and reduces the ratio of charged exciton to neutral excitons. Therefore, the photoluminescence (PL) of both materials was enhanced due to the charge transfer.

The experimental results for PL enhancement for both MoS_2 and WS_2 are similar to the earlier reported photoluminescence of MoS_2 and WS_2 doped with F_4TCNQ from solution[2,5]. In previous studies[2,5], mechanical exfoliated MoS_2 and WS_2 were used. Mechanical exfoliation is the easiest and the fastest method to obtain monolayers of MoS_2 and WS_2. However, only a small portion of MoS_2 and WS_2 crystals are exfoliate to monolayers, leaving a majority of samples as thicker flakes. In this study, we used the chemical vapor deposition to obtain large-area, high-quality monolayers of MoS_2 and WS_2. Therefore, after the F_4TCNQ deposition, our photoluminescence intensity of WS_2 and MoS_2 is approximately fifty times and ten times higher, respectively. Compared to

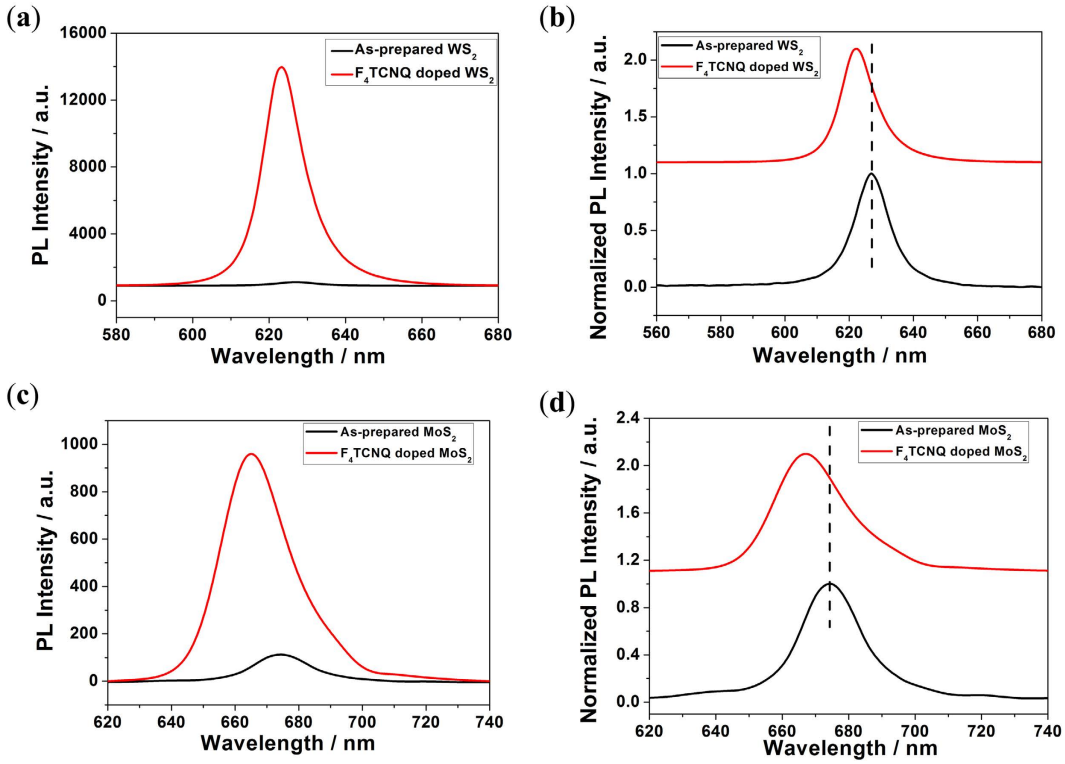

Figure 3. PL spectra of monolayer WS_2 (**a**) and monolayer MoS_2 (**c**) before and after F_4TCNQ doping. PL peak shift of monolayer WS_2 (**b**) and monolayer MoS_2 (**d**) before and after F_4TCNQ doping.

the solution-based chemical doping on MoS_2 monolayer[2], the PL increases approximately three times. During the vacuum deposition of F_4TCNQ on MoS_2 monolayer, there is no solvent contamination and interaction between MoS_2 and F_4TCNQ and therefore the PL increases stronger.

The optical properties of MoS_2 and WS_2, especially the photoluminescence, are affected by the number of layers[6,23]. Few-layered MoS_2 and WS_2 have an indirect band gap and show low photoluminescence, while monolayers of MoS_2 and WS_2 have a direct bandgap and strong photoluminescence[23,24]. To understand the effects of charge transfer, the photoluminescence peaks, which are due to the direct band gap transition, have been analyzed by fitting them with photoluminescence from trions and photoluminescence from neutral excitons represented by two Lorentzian functions, as shown in Fig. 5. For the all cases studied, the photoluminescence signal can be decomposed as A and B peaks, but the intensity of the B peak is negligible. The A peak can be further decomposed to trion (X^-) and exciton (X) components. Peak positions from the fitting can be found in Table 1. The exciton binding energy of MoS_2 and WS_2 (1.85 eV and 1.985 eV) was determined in our work. The trion spectral weight I_{X^-}/I_{total} was also calculated and listed in Table 1.

For both WS_2 and MoS_2, the trion spectral weight I_{X^-}/I_{total} decreases after charge transfer, as shown in Table 1. This indicates that the charge transfer significantly decreases the concentration of trions by transferring electrons from the trions into acceptors, thereby enhancing the photoluminescence.

Upon the deposition of F_4TCNQ on the monolayers, the charge transfer reaches a maximum because the trion spectral weight reaches the saturation region at approximately 0.2. We observe that the peaks for the corresponding X^- and X of PL are sharper for WS_2 than for MoS_2. The wider peak width is associated with a stronger coupling strength or a larger Huang-Rhys factor S for a typical semiconductor[25,26], so that we may ascribe the narrower PL peaks for WS_2 samples compared to MoS_2 as indicative of slightly weaker exciton-phonon coupling[27]. After charge transfer to the F_4TCNQ molecules, the peak width change is almost the same. The weaker exciton-phonon scattering of WS_2 results in narrower PL peaks with a larger amplitude.

The DFT calculated electron transferred from MoS_2 and WS_2 to F_4TCNQ was 0.271 and 0.237, respectively. These data are in good agreement with the trion spectral weight data (Table 1). Larger amount of charge transferred causes more trions to be dissociated to excitons, thereby leading to a lower trion spectral weight. The surface dipole is formed due to the charge transferred from MoS_2/WS_2 to F_4TCNQ. The amount of transferred charge can control the intensity and position of PL. The adding electrons to or withdrawing electrons from the 2D monolayer decreases[7–9] or increases (this work) the intensity of PL.

It is worth to notice that a dipoles formed by charge transfer to acceptor deposited directly on 2D semiconductor is comparable to dipoles formed by Helmholtz double layer in a electrolyte double layer transistor (EDLT), where gate is a reference electrode in an ionic organic liquid. In an EDLT, the number of induced charges is in the transistor channel is in the range of 10^{14} $1/cm^2$. It is almost one order of magnitude larger than the charge induced by the layer of dipoles in our experiment, but two orders of magnitude larger than the charge induced

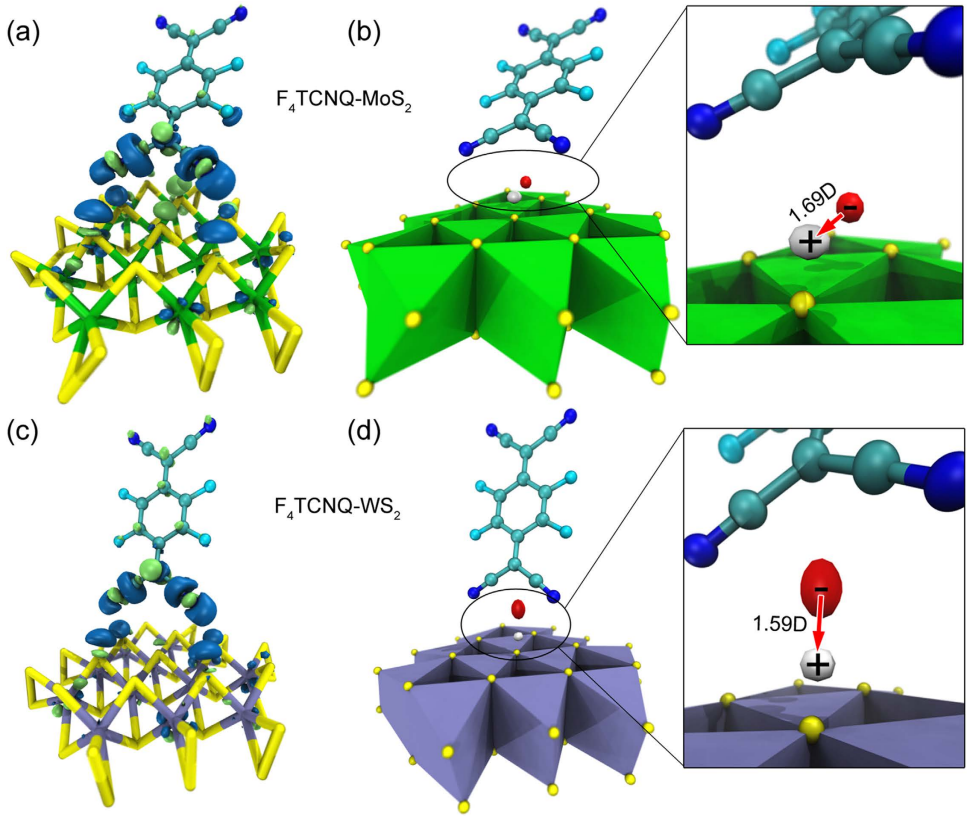

Figure 4. (**a**) Electron density differences (with ± isovalues of 0.005 a.u.) and (**b**) barycenters (with ± isovalues of 0.0001 a.u.) of an F_4TCNQ-doped MoS_2 cluster model. Electron density differences (with ± isovalues of 0.005 a.u.) and barycenters (with ± isovalues of 0.0001 a.u.) for F_4TCNQ-doped WS_2 cluster model are given in (**c**,**d**), respectively. Green and blue isosurfaces indicate positive and negative values in electron density differences, while red and white isosurfaces indicate plus (electron density increase) and minus (electron density depletion) values of barycenters in (**b**,**d**). The dipole moment variation before and after charge transfer are also displayed in the enlarged view of (**c**,**d**), with ± sign indicating virtual charge of the barycenters due to electron density depletion/increase.

in MoS_2 transistor with 280 nm SiO_2 and gate voltage of −70 V[1]. Such high concentration of charge induced in a monolayer of TMD semiconductors should lead to correlated effects like ferromagnetism or to superconductivity in EDLT MoS_2 system[28]. Additionally acceptor layer deposited on the surface on 2D semiconductors can be considered as a stable gate that doesn't required additional connector for gate voltage.

Conclusion

In summary, triangle monolayer WS_2 and MoS_2 were grown using the chemical vapor deposition (CVD) method. The formation of the monolayers was confirmed by both AFM and Raman spectra. The PL increased after a thin layer of F_4TCNQ was deposited on the surface of the WS_2 and MoS_2 monolayers. The ratio of charged excitons, trions, to neutral excitons decreases due to the charge transfer from monolayer WS_2 and MoS_2 to strong acceptor, F_4TCNQ. The weaker exciton-phonon interaction of WS_2 results in narrower PL peaks with larger amplitudes than in MoS_2 where this interaction is strong. Acceptors or donators deposited on the surface of MoS_2 or WS_2 and also on other 2D monolayers provides an effective mechanism for controlling the electron distribution in such heterojunctions. In this way, it is a convenient method of tuning the optoelectronic properties of 2D materials and leads to the application of these materials in lasers or LEDs.

Methods

Chemicals and materials. WO_3 (>99.5%), MoO_3 (>99.5%) and sulfur (>99.95%) powders were purchased from Sigma-Aldrich and used without any purification. F_4TCNQ (>99.5%) was purchased from Jilin OLED Materials Tech. Co. Ltd. and purified at 220 °C via physical vapor transport (PVT).

Preparation of MoS_2 and WS_2 monolayers. For both the triangular shaped MoS_2 and WS_2 monolayers, we used the same method of chemical vapor deposition (CVD). The growth process for the two materials is almost the same, with the only difference being the precursor. Commercially available SiO_2/Si substrates were used in this study. All the substrates were successively cleaned with acetone, methanol, H_2O_2/H_2SO_4 (1 volume/4 volume) and distilled water in an ultrasonic bath for 5 min and then dried in ambient N_2. First, fine WO_3 or MoO_3 powder was spread on the bottom of the crucible. One piece of SiO_2/Si substrate (1 × 1 cm) was

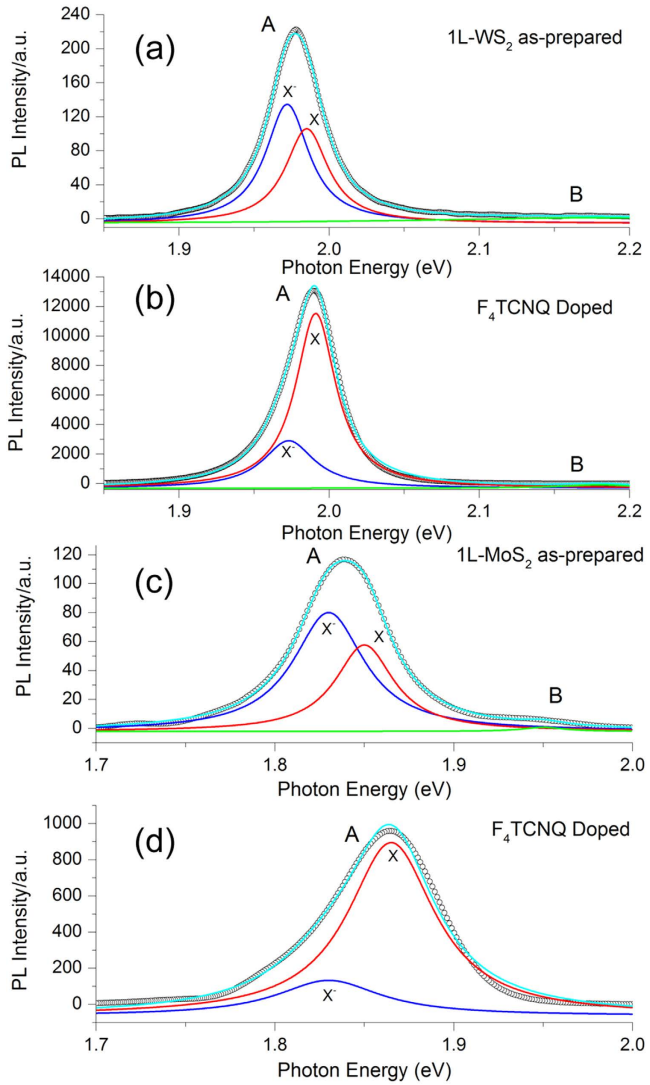

Figure 5. Fitted PL spectra of monolayer WS_2 (**a**) before and (**b**) after F_4TCNQ doping. Fitted PL spectra of monolayer MoS_2 (**c**) before and after F_4TCNQ doping (**d**). Lorentzian functions were used to fit the A and B peaks, with A peaks assumed to be composed of trions (X^-) and excitons (X).

Sample	Peak name	Peak Position (eV)	FWHM(meV)	I_{X^-}/I_{total}
1 L WS_2 as-prepared	X^- trion	1.972 (1.96)	35	0.63
	X exciton	1.985	35	
F_4TCNQ doped 1 L WS_2	X^- trion	1.973 (1.98)	42	0.25
	X exciton	1.991 (2.02)	33	
1 L MoS_2 as-prepared	X^- trion	1.83 (1.84)	48	0.70
	X exciton	1.85 (1.88)	40	
F_4TCNQ doped 1 L MoS_2	X^- trion	1.83 (1.84)	70	0.20
	X exciton	1.865 (1.88)	60	

Table 1. Peak position and width for Lorentzian functions used to fit PL peak A in Fig. 5. (The values in brackets for peak positions were previously reported[2,5]).

placed face-down on the crucible, and the crucible was put in the center of the growth furnace. Another small crucible with approximately 50 mg sulfur powder was put in another part of the furnace near the gas input side at a temperature of 200 °C. The furnace was heated to 750 °C at 25 °C/min and then maintained at that temperature for 20 min before naturally being cooled down to room temperature. Argon gas was provided during the whole growth process at 60 sccm.

Preparation of F_4TCNQ layers on WS_2 and MoS_2 monolayers. 2-nm F_4TCNQ was deposited on the WS_2 and MoS_2 monolayers by the evaporation of F_4TCNQ in a Tectra mini-coater (Germany) with a deposition rate of 0.1 angstrom per second.

Characterization. Photoluminescence was measured at the same area before and after F_4TCNQ deposition. Both the laser beams (solid-state laser, 473 nm and Nd:YAG solid-state laser, 532 nm) were collimated and focused through a ×100 objective onto the sample surface. All the spectra were collected using a confocal triple-grating spectrometer (Horiba-JY T64000). Raman spectra were recorded using a Renishaw Raman microscope configured with a charge-coupled device array detector with the excitation laser line of 532 nm. Atomic force microscopy was performed on a Digital Instruments 3100.

Density functional theory calculations. The geometry of the F_4TCNQ on the surface of the MoS_2/WS_2 was optimized using the DMol^3 [29,30] with the dispersion-corrected (OBS) PW91 (GGA) functional at the level of the DNP basis set. The geometry of the models is regarded as converged when the total energy difference is less than 1×10^{-5} Ha, the total force difference is less than 4×10^{-3} Ha/Å, and the maximum displacement of atoms is less than 5×10^{-3} Å during the optimization. The optimized geometries of the models were subsequently fed into the ORCA 3.0.3 package[31] to perform single-point energy calculations (with SCF convergence criteria set as 1×10^{-6} Ha) at the level of B3LYP/6-31G(d,p) (with Mo and W atoms treated using SDD effective core potentials[32]). To facilitate the charge transfer analysis, the MultiWFN 3.3.7 package[33] was used to calculate the charge transfer based on electron density difference.

References

1. Mak, K. F. *et al.* Tightly bound trions in monolayer MoS_2. *Nat. Mater.* **12,** 207–211 (2013).
2. Mouri, S., Miyauchi, Y. & Matsuda, K. Tunable Photoluminescence of Monolayer MoS_2 via Chemical Doping. *Nano Lett.* **13,** 5944–5948 (2013).
3. Newaz, A. K. M. *et al.* Electrical control of optical properties of monolayer MoS_2. *Solid State Commun.* **155,** 49–52 (2013).
4. Tongay, S. *et al.* Broad-Range Modulation of Light Emission in Two-Dimensional Semiconductors by Molecular Physisorption Gating. *Nano Lett.* **13,** 2831–2836 (2013).
5. Peimyoo, N. *et al.* Chemically Driven Tunable Light Emission of Charged and Neutral Excitons in Monolayer WS_2. *ACS Nano* **8,** 11320–11329 (2014).
6. Dhall, R. *et al.* Direct Bandgap Transition in Many-Layer MoS_2 by Plasma-Induced Layer Decoupling. *Adv. Mater.* **27,** 1573–1578 (2015).
7. Li, Z. *et al.* Active Light Control of the MoS_2 Monolayer Exciton Binding Energy. *ACS Nano* **9,** 10158–10164 (2015).
8. Li, Z. *et al.* Graphene Quantum Dots Doping of MoS_2 Monolayers. *Adv. Mater.* **27,** 5235–5240 (2015).
9. Kang, Y. *et al.* Plasmonic Hot Electron Induced Structural Phase Transition in a MoS_2 Monolayer. *Adv. Mater.* **26,** 6467–6471 (2014).
10. Peimyoo, N. *et al.* Nonblinking, Intense Two-Dimensional Light Emitter: Monolayer WS_2 Triangles. *ACS Nano* **7,** 10985–10994 (2013).
11. Salehzadeh, O., Tran, N. H., Liu, X., Shih, I. & Mi, Z. Exciton Kinetics, Quantum Efficiency, and Efficiency Droop of Monolayer MoS_2 Light-Emitting Devices. *Nano Lett.* **14,** 4125–4130 (2014).
12. Lee, Y.-H. *et al.* Synthesis of Large-Area MoS_2 Atomic Layers with Chemical Vapor Deposition. *Adv. Mater.* **24,** 2320–2325 (2012).
13. Zhan, Y., Liu, Z., Najmaei, S., Ajayan, P. M. & Lou, J. Large-Area Vapor-Phase Growth and Characterization of MoS_2 Atomic Layers on a SiO_2 Substrate. *Small* **8,** 966–971 (2012).
14. Najmaei, S. *et al.* Vapour phase growth and grain boundary structure of molybdenum disulphide atomic layers. *Nat. Mater.* **12,** 754–759 (2013).
15. Zhang, Y. *et al.* Controlled Growth of High-Quality Monolayer WS_2 Layers on Sapphire and Imaging Its Grain Boundary. *ACS Nano* **7,** 8963–8971 (2013).
16. Berkdemir, A. *et al.* Identification of individual and few layers of WS_2 using Raman Spectroscopy. *Sci. Rep.* **3,** 1755 (2013).
17. Huo, N. *et al.* Interlayer coupling and optoelectronic properties of ultrathin two-dimensional heterostructures based on graphene, MoS_2 and WS_2. *J. Mater. Chem. C* **3,** 5467–5473 (2015).
18. Wang, X. H. *et al.* Photoluminescence and Raman mapping characterization of WS_2 monolayers prepared using top-down and bottom-up methods. *J. Mater. Chem. C* **3,** 2589–2592 (2015).
19. Gutiérrez, H. R. *et al.* Extraordinary Room-Temperature Photoluminescence in Triangular WS_2 Monolayers. *Nano Lett.* **13,** 3447–3454 (2013).
20. Zhang, W. *et al.* High-Gain Phototransistors Based on a CVD MoS_2 Monolayer. *Adv. Mater.* **25,** 3456–3461 (2013).
21. Nan, H. *et al.* Strong Photoluminescence Enhancement of MoS_2 through Defect Engineering and Oxygen Bonding. *ACS Nano* **8,** 5738–5745 (2014).
22. Le Bahers, T., Adamo, C. & Ciofini, I. A Qualitative Index of Spatial Extent in Charge-Transfer Excitations. *J. Chem. Theory Comput.* **7,** 2498–2506 (2011).
23. Mak, K. F., Lee, C., Hone, J., Shan, J. & Heinz, T. F. Atomically Thin MoS_2: A New Direct-Gap Semiconductor. *Phys. Rev. Lett.* **105,** 136805 (2010).
24. Splendiani, A. *et al.* Emerging Photoluminescence in Monolayer MoS_2. *Nano Lett.* **10,** 1271–1275 (2010).
25. Chakraborty, B. *et al.* Symmetry-dependent phonon renormalization in monolayer MoS_2 transistor. *Phys. Rev. B* **85,** 161403 (2012).
26. Ye, J., Zhao, Y., Ng, N. & Cao, J. Width of Phonon Sidebands in the Brownian Oscillator Model. *J. Phys. Chem. B* **113,** 5897–5904 (2009).
27. Ho, C. H., Wu, C. S., Huang, Y. S., Liao, P. C. & Tiong, K. K. Temperature dependence of energies and broadening parameters of the band-edge excitons of $Mo_{1-x}W_xS_2$ single crystals. *J. Phys. Condens. Matter* **10,** 9317–9328 (1998).
28. Ye, J. T. *et al.* Superconducting Dome in a Gate-Tuned Band Insulator. *Science* **338,** 1193–1196 (2012).
29. Delley, B. An all-electron numerical method for solving the local density functional for polyatomic molecules. *J. Chem. Phys.* **92,** 508–517 (1990).
30. Delley, B. From molecules to solids with the DMol^3 approach. *J. Chem. Phys.* **113,** 7756–7764 (2000).
31. Neese, F. The ORCA program system. *Wiley Interdiscip. Rev. Comput. Mol. Sci.* **2,** 73–78 (2012).
32. Andrae, D., Häußermann, U., Dolg, M., Stoll, H. & Preuß, H. Energy-adjustedab initio pseudopotentials for the second and third row transition elements. *Theoret. Chim. Acta* **77,** 123–141 (1990).
33. Lu, T. & Chen, F. Multiwfn: A multifunctional wavefunction analyzer. *J. Comput. Chem.* **33,** 580–592 (2012).

Acknowledgements

This research was conducted by the NTU-HUJ-BGU Nanomaterials for Energy and Water Management Programme under the Campus for Research Excellence and Technological Enterprise (CREATE), which is supported by the National Research Foundation, Prime Minister's Office, Singapore. Z.L. thanks Singapore National Research Foundation for NRF RF Award No. NRF-RF2013-08 and the start-up funding from Nanyang Technological University (M4081137.070). Q.X. and C.K. gratefully thanks Singapore Ministry of Education for the strong support via an AcRF tier2 grant (MOE2012-T2-2-086) and AcRT RG125/4 grant. J.Y. would like to thank the support from the Institute of High Performance Computing, Agency for Science, Technology and Research, Singapore.

Author Contributions

P.H., X.H., H.J., Z.L. and C.K. conceived the experiments. P.H. and X.H. performed the experiments including monlayers growth, characterization and data analysis. K.D., K.K.Z., X.W. and Q.X. performed the PL measurement. J.Y. performed all theoretical calculations and wrote respective discussions. J.Y. also prepared Fig. 4 and assist fitting of Fig. 5 and preparation of Table 1. P.H., X.H., H.J. and C.K. co-wrote the manuscript. Z.L., H.J. and C.K. supervised the project. All of the authors reviewed the manuscript, discussed the data and gave profound suggestions.

Additional Information

Supplementary information accompanies this paper at http://www.nature.com/srep

Competing financial interests: The authors declare no competing financial interests.

How to cite this article: Hu, P. *et al.* Control of Radiative Exciton Recombination by Charge Transfer Induced Surface Dipoles in MoS_2 and WS_2 Monolayers. *Sci. Rep.* **6**, 24105; doi: 10.1038/srep24105 (2016).

SCIENTIFIC REPORTS

OPEN

Corrigendum: Control of Radiative Exciton Recombination by Charge Transfer Induced Surface Dipoles in MoS_2 and WS_2 Monolayers

Peng Hu, Jun Ye, Xuexia He, Kezhao Du, Keke K. Zhang, Xingzhi Wang, Qihua Xiong, Zheng Liu, Hui Jiang & Christian Kloc

Correction to: *Scientific Reports* https://doi.org/10.1038/srep24105; published online 07 April 2016; updated 05 April 2018

This article contains an error in Figure 2, where the same image was inadvertently shown in both panel (a) and (b). The correct Figure 2 appears below:

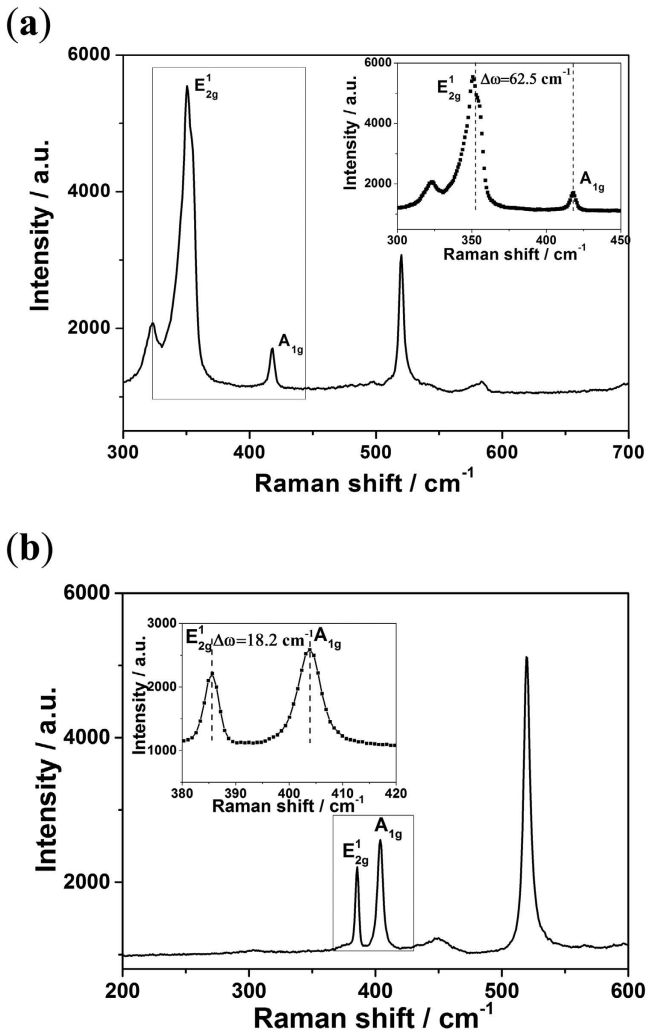

Figure 2.